# *ARCN1* Mutations Cause a Recognizable Craniofacial Syndrome Due to COPI-Mediated Transport Defects

Kosuke Izumi,[1,2,3,*] Maggie Brett,[4] Eriko Nishi,[2,5,6] Séverine Drunat,[7,8] Ee-Shien Tan,[9] Katsunori Fujiki,[1] Sophie Lebon,[7] Breana Cham,[9] Koji Masuda,[1] Michiko Arakawa,[2] Adeline Jacquinet,[10] Yusuke Yamazumi,[11] Shu-Ting Chen,[1] Alain Verloes,[7,8,12] Yuki Okada,[13] Yuki Katou,[1] Tomohiko Nakamura,[6] Tetsu Akiyama,[11] Pierre Gressens,[7,12,14] Roger Foo,[9,15] Sandrine Passemard,[7,8,12] Ene-Choo Tan,[4,16] Vincent El Ghouzzi,[7,12,18] and Katsuhiko Shirahige[1,17,18]

Cellular homeostasis is maintained by the highly organized cooperation of intracellular trafficking systems, including COPI, COPII, and clathrin complexes. COPI is a coatomer protein complex responsible for intracellular protein transport between the endoplasmic reticulum and the Golgi apparatus. The importance of such intracellular transport mechanisms is underscored by the various disorders, including skeletal disorders such as cranio-lenticulo-sutural dysplasia and osteogenesis imperfect, caused by mutations in the COPII coatomer complex. In this article, we report a clinically recognizable craniofacial disorder characterized by facial dysmorphisms, severe micrognathia, rhizomelic shortening, microcephalic dwarfism, and mild developmental delay due to loss-of-function heterozygous mutations in *ARCN1*, which encodes the coatomer subunit delta of COPI. *ARCN1* mutant cell lines were revealed to have endoplasmic reticulum stress, suggesting the involvement of ER stress response in the pathogenesis of this disorder. Given that ARCN1 deficiency causes defective type I collagen transport, reduction of collagen secretion represents the likely mechanism underlying the skeletal phenotype that characterizes this condition. Our findings demonstrate the importance of COPI-mediated transport in human development, including skeletogenesis and brain growth.

In eukaryotic cells, secretory and membrane proteins are generally synthesized on rough endoplasmic reticulum (ER). Vesicle trafficking is required for the correct intracellular transport of these proteins. There are three main intracellular protein trafficking systems: COPI, COPII, and clathrin systems.[1] These transport systems are composed of heteromeric proteins forming a lattice-like protein complex that coats vesicles for intracellular transport. COPI is a heptameric protein complex composed of alpha-COP, beta-COP, beta-prime-COP, gamma-COP, delta-COP, epsilon-COP, and zeta-COP subunits.[1,2] COPI plays an important role in retrograde transport from the Golgi apparatus to the ER; however, recent reports also implicate COPI in anterograde transport from the ER to the Golgi apparatus.[1–3] In order for cells to perform highly complex cellular functions, intracellular transport achieved by COPI plays cardinal roles in cellular homeostasis.

Disruption of intracellular protein transport in human disease has been documented in various genetic disorders. COPII plays major roles in anterograde transport from the ER to the Golgi apparatus,[1] and mutations in COPII components are associated with several genetic disorders. These disorders include lipid absorption disorder (MIM: 246700),[4] skeletal disorders (such as cranio-lenticulo-sutural dysplasia [MIM: 607812][5] and osteogenesis imperfecta [MIM: 616294][6]), hematological disorders (such as congenital dyserythropoietic anemia type II [MIM: 224100][7] and combined deficiency of factor V and factor VIII [MIM: 227300, 613625][8,9]), Cowden syndrome, and thyroid cancer (MIM: 616858).[10] However, in contrast to the findings for COPII, disease-causing germline mutations in COPI components had not been described until lately. Recently, germline mutations of *COPA* encoding the alpha-COP subunit of COPI have been described in individuals with hereditary autoimmune-mediated lung disease and arthritis, demonstrating that the disruption of COPI transport can cause human disease (MIM: 616414).[11] Here, we report a clinically recognizable genetic disorder that we identified in four individuals; this disorder is characterized by facial dysmorphisms, severe micrognathia, rhizomelic shortening, microcephalic dwarfism, and mild developmental delay caused by germline loss-of-function mutations in archain 1 (*ARCN1*), which encodes the coatomer subunit delta of COPI.

[1]Research Center for Epigenetic Disease, Institute of Molecular and Cellular Biosciences, The University of Tokyo, Tokyo 113-0032, Japan; [2]Division of Medical Genetics, Nagano Children's Hospital, Azumino 399-8205, Japan; [3]Division of Human Genetics, The Children's Hospital of Philadelphia, Philadelphia, PA 19104, USA; [4]KK Research Centre, KK Women's and Children's Hospital, Singapore 229899, Singapore; [5]Department of Medical Genetics, Shinshu University Graduate School of Medicine, Matsumoto 390-0802, Japan; [6]Life Science Research Center, Nagano Children's Hospital, Azumino 399-8205, Japan; [7]INSERM UMR1141, Hôpital Robert Debré, Paris 75019, France; [8]Département de Génétique, Hôpital Robert Debré, Paris 75019, France; [9]Genetics Service, Department of Paediatrics, KK Women's and Children's Hospital, Singapore 229899, Singapore; [10]Département de Génétique, Centre Hospitalier Universitaire et Université de Liège, Liège 4000, Belgium; [11]Laboratory of Molecular and Genetic Information, Institute of Molecular and Cellular Biosciences, University of Tokyo, Tokyo 113-0032, Japan; [12]Université Paris Diderot (Paris 7), Hôpital Robert Debré, Paris 75019, France; [13]Laboratory of Pathology and Development, Institute of Molecular and Cellular Biosciences, The University of Tokyo, Tokyo 113-0032, Japan; [14]The Centre for the Developing Brain, King's College London, St. Thomas' Hospital, London SE1-7EH, UK; [15]Genome Institute of Singapore, Singapore 138672, Singapore; [16]Paediatrics ACP, SingHealth Duke-NUS Medical School, Singapore 169857, Singapore; [17]CREST, Japan Science and Technology Agency, Kawaguchi, 332-0012, Japan
[18]These authors contributed equally to this work
*Correspondence: izumik1@email.chop.edu
http://dx.doi.org/10.1016/j.ajhg.2016.06.011.

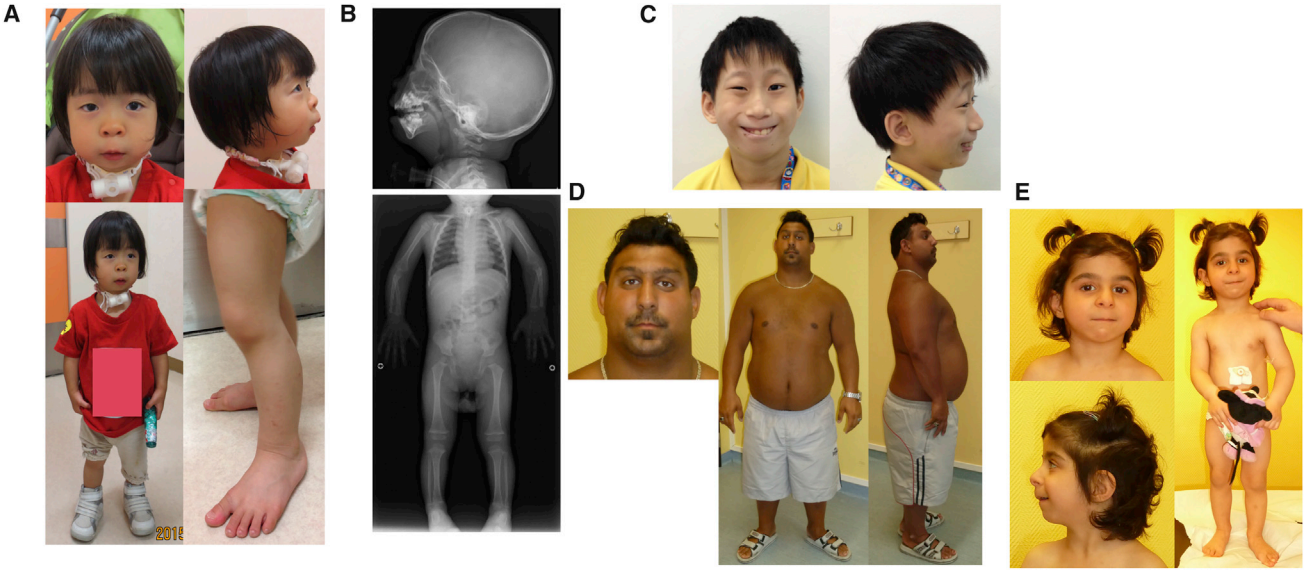


**Figure 1. Clinical Features of the Individuals with *ARCN1* Mutations**
(A) Physical features of subject 1. Note downslanted palpebral fissures and micrognathia.
(B) Skeletal survey of subject 1. Note micrognathia, widening of the metaphysis, and a wide femoral neck.
(C) Facial features of subject 2.
(D) Physical features of subject 3. Note rhizomelic shortening of the limbs.
(E) Physical features of subject 4. Note micrognathia and rhizomelic shortening of the limbs.
The guardians of these individuals provided consent for the publication of their photographs.

Four individuals with *ARCN1* mutations were independently enrolled in our study after approval by the institutional review boards of The University of Tokyo, Nagano Children's Hospital, KK Women's and Children's Hospital, and the genetics departments of the Centre Hospitalier Universitaire and the University of Liège. Informed consent for genetic and molecular studies was obtained from the guardians of the subjects. Shared clinical features among these four individuals are facial dysmorphisms, including severe micrognathia, rhizomelic shortening, and microcephalic dwarfism (see case reports in the Supplemental Note, Figure 1, Table 1). Subject 1 was referred to the genetics clinic of Nagano Children's Hospital at the age of 1 month with the chief complaints of facial dysmorphism and intrauterine growth retardation. On physical examination, several facial dysmorphisms, including a prominent forehead, downslanted palpebral fissures, and severe micrognathia, were noted. In addition, shortening of upper arms and legs and small joint laxity were observed (Figure 1A). A skeletal survey revealed widening of the metaphysis and a wide femoral neck (Figure 1B). Subject 2, a boy with developmental delay and mild autism, was first seen in the genetics clinic at the KK Women's and Children's Hospital at the age of 1 year and 8 months. Subject 2 had micrognathia, scaphocephaly, and hypotelorism, as well as small joint laxity (Figure 1C). The clinical history of subject 3 was partly reported previously by Verloes et al.[12] At the age of 25 years, his weight was 98 kg, his length was 152 cm (−3.5 SD), and his head circumference was 50 cm (−5 SD) (Figure 1D). Subject 4, the daughter of subject 3, shared common features with subject 3, which included intrauterine growth retardation followed by postnatal growth failure (length 79.5 cm, −4 SD), microcephaly (head circumference 45 cm, −5 SD), and dysmorphic features, including microretrognathia, hypotelorism, shortening of upper arms and legs, and muscular hypertrophy (Figure 1E).

Exome sequencing was performed with genomic DNA extracted from peripheral blood cells. Exome sequencing of the probands revealed heterozygous *ARCN1* loss-of-function mutations (Figure 2). Subject 1's mutation in *ARCN1* (GenBank: NM_001655) resulted in a premature stop codon in exon 2 (c. 260C>A [p.Ser87*]). Exome sequencing of subject 2 revealed two de novo mutations in *ARCN1* and *SYT1*. The *ARCN1* mutation was a frameshift variant (c.633del [p.Val212Trpfs*15]) predicted to create a frameshift in exon 4 starting at codon Val212 and ending in a stop codon 14 positions downstream (Figure 2A and Figure S2B). The *SYT1* (c.697G>A [p.Asp233Asn] [GenBank: NM_001135805.1]) variant is a missense variant that substitutes aspartic acid at codon 233 with asparagine (Figure S3C). Subjects 3 and 4 were found to have a common *ARCN1* mutation, c.157_158del, leading to p.Ser53Cysfs*39 (Figure S2C).

In order to evaluate the effect of loss-of-function mutations of *ARCN1*, genome editing was performed with the CRISPR/Cas9 system on the colon-cancer-derived HCT116 cell line. After the introduction of the *ARCN1* mutation into these cells, single-cell cloning was performed with the limiting dilution technique. The gRNA empty vector (catalog no. 41824) and hCas9 vector (41815)

**Table 1. Clinical Features of *ARCN1*-Related Syndrome**

| | Subject 1 | Subject 2 | Subject 3 | Subject 4 |
|---|---|---|---|---|
| IUGR | + | + | + | + |
| Micrognathia | + | + | + | + |
| Cleft palate | − | − | − | + |
| Tracheostomy | + | + | − | − |
| Congenital heart disease | +, VSD | − | − | − |
| Cryptorchidism | NA | + | − | NA |
| Short stature | + | + | + | + |
| Rhizomelic shortening | + | − | + | + |
| Joint laxity | + | + | − | + |
| Developmental delay | + | + | + | + |
| Autism | − | + | − | − |
| Seizure | − | + | − | − |
| Microcephaly | + | − | + | + |
| *ARCN1* mutation | p.Ser87* | p.Val212Trpfs*15 | p.Ser53Cysfs*39 | p.Ser53Cysfs*39 |

+, present; −, absent; IUGR, intrauterine growth retardation; VSD, ventricular septal defect; NA, not applicable.

were obtained from Addgene. The gRNA target sequence was cloned into the gRNA empty vector with Phusion polymerase (M0530S, New England Biolabs) and the Gibson assembly system (E5510S, New England Biolabs). The gRNA target sequence was CTAAGGCTCTTCTCAAGAG; it is located at exon 2 of *ARCN1*. Cas9 and gRNA vectors were transfected into cell lines by electroporation via a Neon electroporation system (ThermoFisher Scientific). Genomic DNA was extracted with NucleoSpin tissue kits (Macherey-Nagel). The presence of the *ARCN1* mutation was confirmed by Sanger sequencing. A total of 68 clones were screened, and 5 clones with *ARCN1* mutations were identified. None of the clones possessed biallelic loss-of-function mutations of *ARCN1*, suggesting the importance of ARCN1 in maintaining cell viability. Two independent clones possessing 1-bp duplication leading to a frameshift that resembled the mutations identified in subject 1 (c.262dupA, in *ARCN1* [GenBank: NM_001655]) were used for subsequent experiments (Figure S2D). Analysis with the ExPASy Translate tool indicated that this 1-bp duplication leads to p.Arg88Lysfs*5. Similar to the mutation found in four individuals with *ARCN1* mutations, this frameshift mutation in the HCT116 cell line likely causes a loss-of-function effect, given that the mRNA in the case of this 1-bp insertion is predicted to undergo nonsense-mediated decay.

To test whether such a truncating mutation caused actual dosage reduction of ARCN1, we quantified *ARCN1* mRNA by using qRT-PCR. Introduction of frameshift mutations in exon 2 resulted in reduction in *ARCN1* mRNA expression, confirming that truncating mutations cause a reduction in the expression of the *ARCN1* transcript (Figure 2B). Reduction of *ARCN1* mRNA expression was also observed in the skin fibroblast samples obtained from subjects 3 and 4 (Figure S4A).

In order to test the amount of ARCN1, HCT116 cells with and without *ARCN1* mutations were lysed with SDS sample buffer for immunoblotting. Western blotting of HCT116 mutant clones showed a reduction of ARCN1, in comparison to that in the wild-type clones (Figure 2C). Mild reduction of ARCN1 was also demonstrated in the skin fibroblast sample obtained from subject 4 (Figure S4B). These observations confirmed that truncating mutations of *ARCN1* cause reduction of *ARCN1* mRNA and protein amounts.

Given the phenotypic overlap of the individuals with *ARCN1* mutations and individuals with collagenopathies such as Stickler syndrome (MIM: 108300), we hypothesized that reduction of ARCN1 might have caused intracellular collagen transport defects. To evaluate the effect of loss-of-function *ARCN1* mutations, siRNA-mediated gene knockdown (KD) of *ARCN1* was performed on a control skin fibroblast cell line, GM02036, given that skin fibroblast cell lines synthesize type I collagen.[13,14] The greatest reduction in *ARCN1* mRNA and ARCN1 protein amounts was achieved 4 days after *ARCN1* KD (Figure 3A and Figure 4A).

Disruption of intracellular trafficking can cause the accumulation of protein, leading to an ER stress response. When the rate of protein synthesis exceeds the capacity of protein folding and protein degradation machinery, the ER stress response is induced, which can result in cell death if prolonged.[15] Therefore, the degree of the ER stress response was evaluated in the skin fibroblast cell line after *ARCN1* KD. Overexpression of stress response genes such as *ATF4*, *DDIT3*, and *HSPA5* serves as a marker of ER stress.

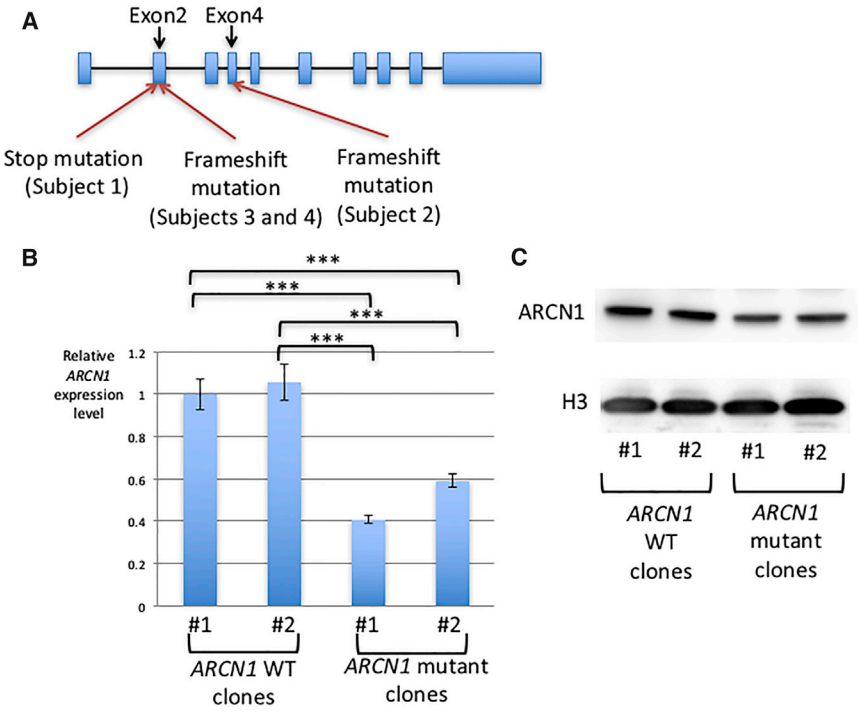


**Figure 2. Effects of *ARCN1* Mutation**

(A) Structure of *ARCN1* (GenBank: NM_001655) and the location of *ARCN1* mutations identified. Subject 1 has a stop mutation in exon 2, c. 260C>A (p.Ser87*). Subject 2 has a frameshift mutation in exon 4, c.633del (p.Val212Trpfs*15). Subjects 3 and 4 have a common *ARCN1* mutation in exon 2, c.157_158del (p.Ser53Cysfs*39).

(B) mRNA expression of *ARCN1* in HCT116 cell lines with and without *ARCN1* mutation. RNA extraction was performed with TRIzol reagent (15596-018, Ambion) and Nucleospin RNA kits (Macherey-Nagel). The RNA obtained was reverse transcribed with a SuperScript VILO cDNA Synthesis Kit (11754-050, Invitrogen). The PCR primer sets used for qRT-PCR are listed in Table S2. *ARCN1* expression was normalized against *GAPDH*. *ARCN1* expression relative to that of the control sample (WT #1) is demonstrated. Data represent mean ± 2 SD. ***$p < 0.001$, two-tailed t test. $n = 3$ technical replicates per group. Three biological replicates for each sample demonstrated consistent results. WT, wild-type.

(C) Amounts of ARCN1 in HCT116 cell lines with and without *ARCN1* mutation. The ARCN1 antibody (ab96725) and histone H3 antibody (ab1791) were from Abcam. Three biological replicates for each sample demonstrated consistent results.

qRT-PCR analysis demonstrated the upregulation of all these ER stress response genes after *ARCN1* KD (Figure 3B). Therefore, reduction in ARCN1 amounts triggered the ER stress response. In order to evaluate the consequence of ER stress, cells were treated with thapsigargin (2 μM and 5 μM)[16] and tunicamycin (2 μg/mL and 5 μg/mL)[17,18] for 17 hr; then, the total cellular lysates and RNA were obtained. Thapsigargin is an inhibitor of the ER $Ca^{2+}$ATPase and induces ER stress, and tunicamycin inhibits the initial step of glycoprotein synthesis in the ER and induces ER stress. Artificial induction of ER stress by the addition of thapsigargin and tunicamycin triggered *ARCN1* overexpression, although the amount of ARCN1 remained unchanged, suggesting increased ARCN1 turnover during the ER stress response (Figures 5A and 5B). Collectively, these results suggest that ARCN1 plays a major role in ameliorating the induction of the ER stress response. Evaluation of the skin fibroblast sample from subject 4 further confirmed the presence of ER stress, indicated by the cytosolic accumulation of BiP, which is an ER stress marker (Figures S4C and S5). Therefore, reduction in the amount of ARCN1 triggered the ER stress response.

Next, the amount of type I collagen was evaluated in the control skin fibroblasts with *ARCN1* KD. Interestingly, *ARCN1* KD caused the accumulation of type I collagen in the total cellular lysates (Figure 4A). Type I collagen secretion from skin fibroblasts was then quantitated by performing trichloroacetic acid (TCA) precipitation of culture supernatants. Immunoblotting performed on culture supernatants demonstrated the reduction of secreted type I collagen in the culture media, suggesting that ARCN1 reduction caused intracellular accumulation of type I collagen as a result of defective intracellular protein transport (Figure 4A). In order to confirm that collagen accumulation was a result of defective intracellular transport, 10 μM brefeldin A (BFA), an ER-Golgi transport inhibitor, was added to the culture media, and total cellular lysates were obtained 23 hr after treatment.[18] Addition of BFA caused the accumulation of intracellular type I collagen, similar to what was observed with *ARCN1* KD (Figure 4B). Interestingly, BFA treatment reduced the amount of ARCN1 in the cells (Figure 4B). Type I collagen is encoded by two genes, *COL1A1* and *COL1A2*. The alpha 1 chain of type I collagen is encoded by *COL1A1*, and the alpha 2 chain of type I collagen is encoded by *COL1A2*. qRT-PCR demonstrated a slight reduction in *COL1A1* mRNA with *ARCN1* KD, whereas the expression of *COL1A2* mRNA remained unchanged with *ARCN1* KD (Figure 4C). The addition of thapsigargin and tunicamycin did not cause accumulation of type I collagen, suggesting that the ER stress response does not cause the collagen transport defect (Figure 5B and Figure S6). These experiments indicate that ARCN1 is directly responsible for the intracellular transport of type I collagen and that the collagen transport defect is not secondary to the ER stress response.

In this paper, we report a clinically recognizable genetic disorder characterized by facial dysmorphisms, micrognathia, rhizomelic shortening, microcephalic dwarfism, and mild intellectual disability due to heterozygous *ARCN1* loss-of-function mutations. We propose the name "*ARCN1*-related syndrome" to denote this condition. The *ARCN1* is approximately 30 kb in size and located on

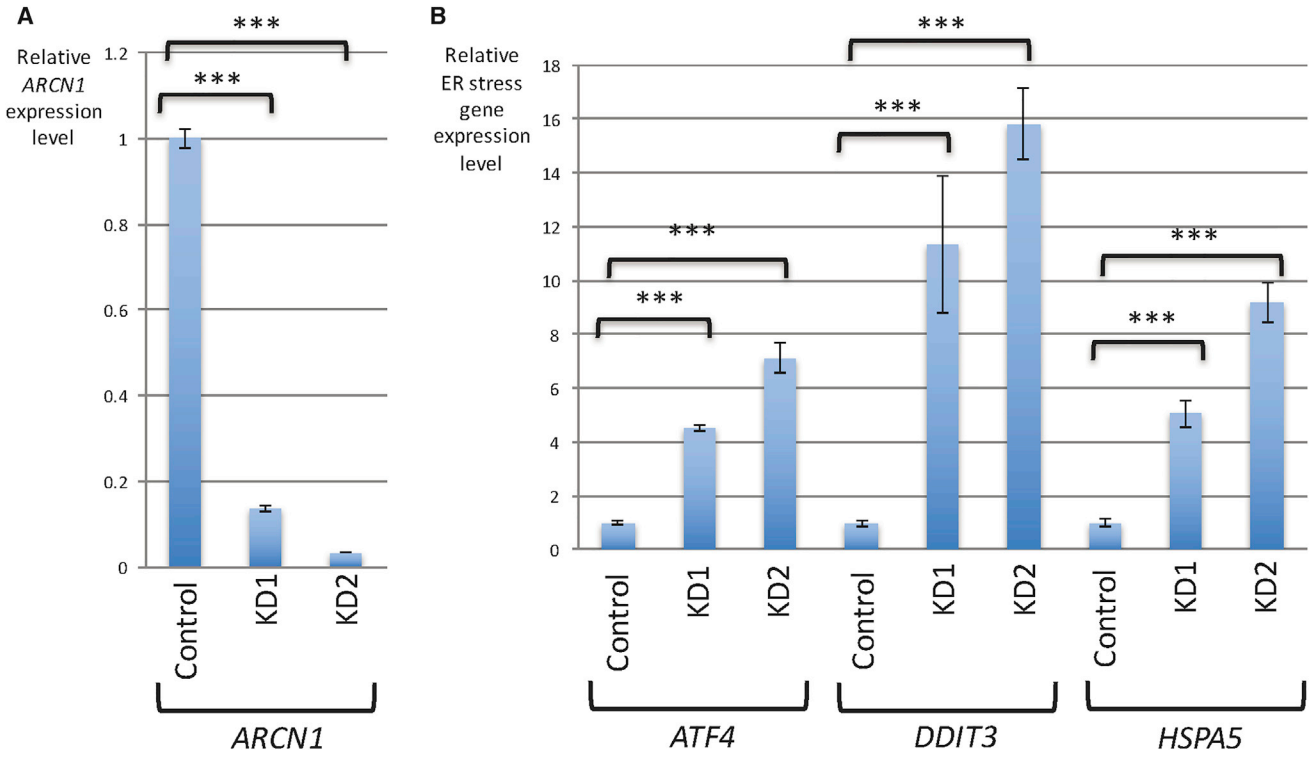


**Figure 3. ER Stress Response with the Reduction of ARCN1**

Skin fibroblast *ARCN1*-KD experiments were performed three times, and consistent results were obtained. Two different siRNAs (ARCN1HSS100628 [KD1] and ARCN1HSS100629 [KD2], ThermoFisher Scientific) were used in the study. Stealth siRNA was transfected with Lipofectamine RNAiMAX reagent (ThermoFisher Scientific), according to the manufacturer's instructions. For *ARCN*- KD in skin fibroblasts, two siRNA transfections were performed 2 days apart; 4 days after the initial siRNA transfection, RNA and cellular lysates were harvested.

(A) *ARCN1* mRNA expression with *ARCN1* KD. qPCR was run in triplicates, and mean and SD were calculated. *ARCN1* expression was normalized against *GAPDH* expression. Gene expression relative to that of the control sample is shown. Data represent mean ± 2 SD. ***$p < 0.001$, two-tailed t test. $n = 3$ technical replicates per group.

(B) Elevation of ER stress response genes' expression upon *ARCN1* KD. Gene expression was normalized against *GAPDH* expression. Gene expression relative to that of the control sample is shown. Data represent mean ± 2 SD. ***$p < 0.001$, two-tailed t test. $n = 3$ technical replicates per group.

chromosomal region 11q23.3 with ten exons (Figure 2A). Germline mutations of *ARCN1* have not been previously reported. The Exome Aggregation Consortium (ExAC) website gives a probability of loss-of-function intolerance score of 1 to *ARCN1*, the highest score, given the absence of loss-of-function *ARCN1* mutations in their cohort.[19] Therefore, *ARCN1* likely represents a dosage-sensitive gene in humans. To the best of our knowledge, germline chromosomal microdeletions spanning the *ARCN1* region have not been reported in the medical literature. Copy-number variations within the *ARCN1* locus have also not been reported in the Database of Genomic Variants.

The clinical phenotype of *ARCN1*-related syndrome includes severe micrognathia, microcephalic dwarfism, joint laxity, and mild developmental delay (Table 1). There is some phenotypic overlap between *ARCN1*-related syndrome and Stickler syndrome, such as micrognathia, short stature, and joint laxity, although neurological, ocular, and audiology features differ. Stickler syndrome is caused by loss-of-function heterozygous mutations in *COL2A1* and other collagen genes.[20] Given the type of the mutations identified in Stickler syndrome, it is presumed that generalized reduction in type II collagen production leads to a clinical phenotype of Stickler syndrome, including features such as micrognathia and short stature. This clinical overlap prompted us to evaluate the role of ARCN1 in intracellular collagen transport, where we demonstrated the importance of ARCN1. Phenotypic resemblance between *ARCN1*-related syndrome and Stickler syndrome could be explained by the reduction in collagen secretion from the cells. The importance of ARCN1-associated intracellular trafficking has been documented in many biological processes, such as immune function and influenza virus infection.[21] The inability to create an *ARCN1*-null cell line with CRISPR/Cas9 underscores the importance of ARCN1 in cell viability. Our findings highlight the unexpected importance of COPI transport in skeletogenesis, particularly in mandibular bone formation. Previously, similar pathological disease mechanisms resulting in skeletal dysplasia were implicated in COPII transport defects, such as cranio-lenticulo-sutural dysplasia and osteogenesis imperfecta.[6,22]

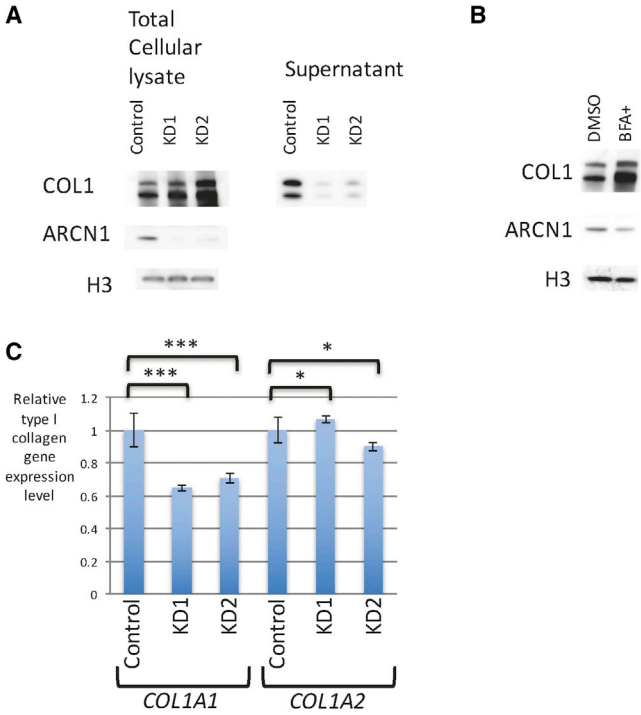


**Figure 4. Collagen Transport Defects with *ARCN1* KD**
(A) Reduction of ARCN1 caused accumulation of type I collagen in total cellular lysates and reduction of type I collagen secretion. The type I collagen antibody (AB758) was from Millipore.[13] For the measurement of culture supernatant type I collagen, skin fibroblast cell numbers were counted, and equal numbers were plated in culture flasks. The cells were changed to serum-free culture media for the final 24 hr, the time point at which the medium was harvested. One-tenth the volume of TCA was added and placed on ice for 30 min. The samples were centrifuged and precipitates were washed with ethanol. After the ethanol wash, the supernatants were dried and the remaining cell pellets were dissolved with SDS sample buffer for immunoblotting. TCA precipitation was performed four times, and consistent results were obtained. Two bands of type I collagen represent the bands for alpha 1 and alpha 2 type I collagen. Top larger band represents alpha 1 type I collagen, and lower smaller band represents alpha 2 type I collagen.
(B) Brefeldin A (BFA; B5936, Sigma-Aldrich) treatment caused the intracellular accumulation of type I collagen. 10 uM of BFA was used. DMSO was added for control. The BFA treatment experiment was performed three times, and consistent results were obtained.
(C) *COL1A1* and *COL1A2* expression with *ARCN1* KD. Slight reduction of *COL1A1* expression was elicited with *ARCN1* KD; however, the expression of *COL1A2* remained unchanged. Gene expression was normalized against *GAPDH* expression. Gene expression relative to that of the control sample is shown. Data represent mean ± 2 SD. *p < 0.05, ***p < 0.001, two-tailed t test. n = 3 technical replicates per group.

*COL2A1* mutations also cause other skeletal dysplasias, such as achondrogenesis type II or hypochondrogenesis (MIM: 200610) and spondyloepiphyseal dysplasia (MIM: 183900). These disorders are collectively termed type II collagenopathies.[23] Many of these conditions are caused by heterozygous mutations in *COL2A1*. However, the effects of *COL2A1* mutations vary in different type II collagenopathies. As a result, there is a wide phenotypic spectrum of type II collagenopathies. Interestingly, some *COL2A1* missense mutations found in type II collagenopathies cause abnormal protein folding of type II collagen, leading to the intracellular accumulation of mutant collagen, which elicits an ER stress response.[24] Furthermore, the artificial induction of ER stress in chondrocytes causes skeletal dysplasia in mice.[25] Therefore, it is proposed that ER stress itself is involved in the pathogenesis of skeletal dysplasia. Hence, in *ARCN1*-related syndrome, the ER stress response might also play a role in the resultant skeletal phenotype. However, our *ARCN1*-KD experiments indicate that defective COPI transport could play a direct role in intracellular collagen accumulation in *ARCN1*-related syndrome, rather than the skeletal phenotype, which is secondary to ER stress. This finding is consistent with a previous report that demonstrated the involvement of COPI in intracellular collagen transport.[26] In order to deepen the understanding of the role that ER stress and COPI transport play in skeletogenesis, further studies are warranted.

The ER stress response is elicited even during normal embryogenesis.[27,28] Given the role of ARCN1 in the ER stress response, reduction of ARCN1 likely triggers an exaggerated ER stress response, and such an enhanced ER stress response might lead to cell death. In addition to the direct influence of ER-Golgi transport defects secondary to *ARCN1* mutations, such cell death most likely contributes to the pleiotropic phenotype of *ARCN1*-related syndrome.

Mice with a homozygous missense mutation in *Arcn1*, that is, nur17 mice, have been previously created by N-ethyl-N-nitrosourea (ENU) mutagenesis.[29] The nur17 mouse harbors a homozygous missense mutation in exon 10 of *Arcn1* and is characterized by the presence of dilute coat color, neurological defects, and low body weight; however, the skeletal phenotype was not characterized in the original report. Mild loss-of-function effects were presumed to mediate disease mechanisms in the nur17 mutant mouse. There are several similarities between *Arcn1* mutant mice and the individuals with *ARCN1*-related syndrome, such as low body weight and the neurological phenotype, including ataxia due to cerebellar degeneration. Interestingly, subject 4 was found to have ataxia and cerebellar atrophy. Hence, nur17 mice might serve as an animal model for *ARCN1*-related syndrome, although skin color and hair abnormalities were not detected in individuals with *ARCN1* mutations.

In addition to the skeletal phenotype, another feature typical of *ARCN1*-related syndrome is mild intellectual disability. There are several lines of evidence supporting a role for COPI transport in brain function. First, COPI interacts with a subset of RNA molecules, and COPI has been implicated in intracellular RNA transport in neuronal cells.[30] Second, the COPI system is known to transport molecules that play major roles in neurotransmitter release, such as SNARE proteins.[31–33] In fact, the importance of intracellular trafficking has been well known in neuronal function and homeostasis because the abnormalities of intracellular trafficking are linked to the pathogenesis of various neurodegenerative disorders, such as

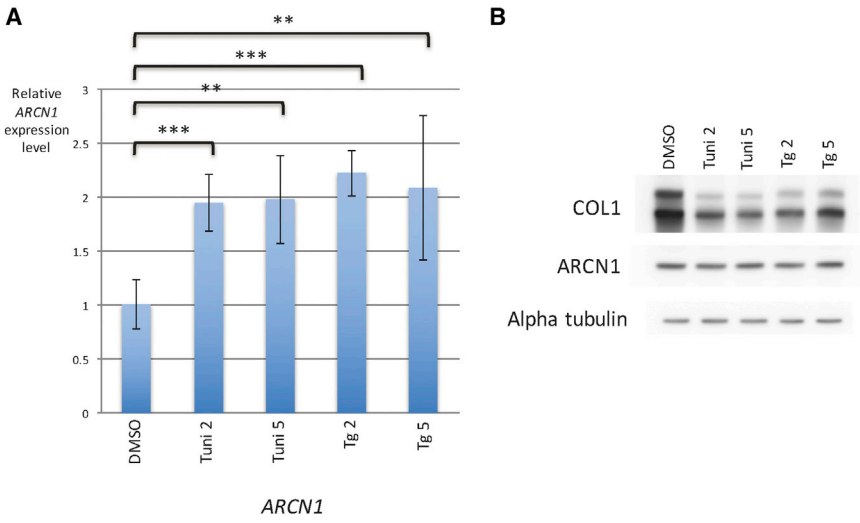


**Figure 5. Artificial Induction of ER Stress Caused *ARCN1* mRNA Overexpression**
(A) Treatment with tunicamycin (T7765, Sigma-Aldrich) and thapsigargin (T9033, Sigma-Aldrich) triggered overexpression of *ARCN1*. *ARCN1* expression was normalized against *GAPDH* expression. Gene expression relative to that of the control sample is shown. Data represent mean ± 2 SD. **$p < 0.01$, ***$p < 0.001$, two-tailed t test. $n = 3$ technical replicates per group. (B) The amount of ARCN1 remained unchanged with tunicamycin and thapsigargin treatments. The alpha tubulin antibody (T6074) was from Sigma-Aldrich. Two different concentrations of tunicamycin treatment (2 μg/mL [Tuni2] and 5 μg/mL [Tuni5]) and thapsigargin treatment (2 μM [Tg2] and 5 μM [Tg5]) were used. DMSO was added for control. Two biological replicates demonstrated the consistent results.

Alzheimer disease.[34] Abnormal ER-Golgi trafficking is demonstrated in Dyggve-Melchior-Clause syndrome (MIM: 223800), associated with developmental delay and microcephaly.[35] Furthermore, the presence of ER stress during embryogenesis is well documented in the CNS, supporting a role for ER stress in brain development.[27,28] Therefore, the findings strongly suggest that COPI is involved in neuronal function. The neurological phenotype of the nur17 mouse model further supports the notion that defective ARCN1 function impairs brain function.[29]

Subject 2 experienced seizures in addition to intellectual disability. However, it remains to be determined whether the seizures were due to *ARCN1* mutations given that subject 2 also has a de novo missense *SYT1* variant, which was not previously reported. *SYT1* encodes synaptotagmin-1, which plays important roles in synaptic vesicle recycling, and there have been two recent reports associating *SYT1* mutations with dyskinetic movement disorder and developmental delay in one child and with developmental delay, facial dysmorphisms, and anomalous electroencephalogram (EEG) patterns in another child[36,37] (Table S3). Therefore, it is possible that the neurological phenotype of subject 2 is partially due to the *SYT1* mutation. However, given that all four individuals with *ARCN1* mutations demonstrated comparable degrees of developmental delay and intellectual disability, *ARCN1* mutations most likely play a major role in the neurological phenotype of *ARCN1*-related syndrome, and ARCN1 is probably required for normal brain growth and cognitive development.

In conclusion, we report a recognizable craniofacial disorder, *ARCN1*-related syndrome, characterized by facial dysmorphisms, micrognathia, rhizomelic shortening, microcephalic dwarfism, and mild intellectual disability. Intracellular COPI transport has been implicated in various biological processes, and our results strongly indicate the importance of COPI transport in skeletogenesis, particularly in mandibular bone formation, during embryogenesis.

## Supplemental Data

Supplemental Data include a Supplemental Note, six figures, and three tables and can be found with this article online at http://dx.doi.org/10.1016/j.ajhg.2016.06.011.

## Acknowledgments

The authors greatly appreciate the family members of the probands for their participation in our research study. We thank Keiko Nakagawa, Masashi Minamino, and Kazuhiro Akiyama for their technical assistance and Dagmar Wieczorek and Elizabeth Bhoj for sharing their research cohort information. *ARCN1* was submitted as a candidate gene to GeneMatcher by three independent research groups in Japan, Singapore, and France.[38] The authors appreciate the GeneMatcher website for facilitating the collaboration. This work was supported by a Grant-in-Aid for Scientific Research (15H02369 and 15H05976 to K.S.) from MEXT and AMED-CREST from AMED; NMRC/PPG/KKH12010-Theme3 and NMRC/CG/006/2013 from the National Medical Research Council, Ministry of Health, Republic of Singapore; two Programmes Hospitaliers de Recherche Clinique (PHRC) grants from the French Ministry of Health (P100128 / IDRCB: 2010-A01481-38 and HAO11011/ ExoMicro: NI11016); and a European ERA-NET grant for research on rare diseases (ANR-13-RARE-0007-01 2013).

Received: March 3, 2016
Accepted: June 15, 2016
Published: July 28, 2016

## Web Resources

Database of Genomic Variants (DGV), http://dgv.tcag.ca/dgv/app/home
ExAC Browser, http://exac.broadinstitute.org/
ExPASy Translate tool, http://web.expasy.org/translate/
GenBank, http://www.ncbi.nlm.nih.gov/genbank/

GeneMatcher, https://genematcher.org/
OMIM, http://www.omim.org/

## References


1. Faini, M., Beck, R., Wieland, F.T., and Briggs, J.A.G. (2013). Vesicle coats: structure, function, and general principles of assembly. Trends Cell Biol. *23*, 279–288.
2. Jackson, L.P. (2014). Structure and mechanism of COPI vesicle biogenesis. Curr. Opin. Cell Biol. *29*, 67–73.
3. Park, S.-Y., Yang, J.-S., Schmider, A.B., Soberman, R.J., and Hsu, V.W. (2015). Coordinated regulation of bidirectional COPI transport at the Golgi by CDC42. Nature *521*, 529–532.
4. Jones, B., Jones, E.L., Bonney, S.A., Patel, H.N., Mensenkamp, A.R., Eichenbaum-Voline, S., Rudling, M., Myrdal, U., Annesi, G., Naik, S., et al. (2003). Mutations in a Sar1 GTPase of COPII vesicles are associated with lipid absorption disorders. Nat. Genet. *34*, 29–31.
5. Boyadjiev, S.A., Fromme, J.C., Ben, J., Chong, S.S., Nauta, C., Hur, D.J., Zhang, G., Hamamoto, S., Schekman, R., Ravazzola, M., et al. (2006). Cranio-lenticulo-sutural dysplasia is caused by a SEC23A mutation leading to abnormal endoplasmic-reticulum-to-Golgi trafficking. Nat. Genet. *38*, 1192–1197.
6. Garbes, L., Kim, K., Rieß, A., Hoyer-Kuhn, H., Beleggia, F., Bevot, A., Kim, M.J., Huh, Y.H., Kweon, H.-S., Savarirayan, R., et al. (2015). Mutations in SEC24D, encoding a component of the COPII machinery, cause a syndromic form of osteogenesis imperfecta. Am. J. Hum. Genet. *96*, 432–439.
7. Schwarz, K., Iolascon, A., Verissimo, F., Trede, N.S., Horsley, W., Chen, W., Paw, B.H., Hopfner, K.-P., Holzmann, K., Russo, R., et al. (2009). Mutations affecting the secretory COPII coat component SEC23B cause congenital dyserythropoietic anemia type II. Nat. Genet. *41*, 936–940.
8. Nichols, W.C., Seligsohn, U., Zivelin, A., Terry, V.H., Hertel, C.E., Wheatley, M.A., Moussalli, M.J., Hauri, H.P., Ciavarella, N., Kaufman, R.J., and Ginsburg, D. (1998). Mutations in the ER-Golgi intermediate compartment protein ERGIC-53 cause combined deficiency of coagulation factors V and VIII. Cell *93*, 61–70.
9. Zhang, B., Cunningham, M.A., Nichols, W.C., Bernat, J.A., Seligsohn, U., Pipe, S.W., McVey, J.H., Schulte-Overberg, U., de Bosch, N.B., Ruiz-Saez, A., et al. (2003). Bleeding due to disruption of a cargo-specific ER-to-Golgi transport complex. Nat. Genet. *34*, 220–225.
10. Yehia, L., Niazi, F., Ni, Y., Ngeow, J., Sankunny, M., Liu, Z., Wei, W., Mester, J.L., Keri, R.A., Zhang, B., and Eng, C. (2015). Germline Heterozygous Variants in SEC23B Are Associated with Cowden Syndrome and Enriched in Apparently Sporadic Thyroid Cancer. Am. J. Hum. Genet. *97*, 661–676.
11. Watkin, L.B., Jessen, B., Wiszniewski, W., Vece, T.J., Jan, M., Sha, Y., Thamsen, M., Santos-Cortez, R.L.P., Lee, K., Gambin, T., et al.; Baylor-Hopkins Center for Mendelian Genomics (2015). COPA mutations impair ER-Golgi transport and cause hereditary autoimmune-mediated lung disease and arthritis. Nat. Genet. *47*, 654–660.
12. Verloes, A., Lesenfants, S., Misson, J.P., Galand, A., and Koulischer, L. (1997). Microcephaly, muscular build, rhizomelia, and cataracts: description of a possible recessive syndrome and some comments on the use of electronic databases in syndromology. Am. J. Med. Genet. *68*, 455–460, discussion 461.
13. Ishikura-Kinoshita, S., Saeki, H., and Tsuji-Naito, K. (2012). BBF2H7-mediated Sec23A pathway is required for endoplasmic reticulum-to-Golgi trafficking in dermal fibroblasts to promote collagen synthesis. J. Invest. Dermatol. *132*, 2010–2018.
14. Izumi, K., Nakato, R., Zhang, Z., Edmondson, A.C., Noon, S., Dulik, M.C., Rajagopalan, R., Venditti, C.P., Gripp, K., Samanich, J., et al. (2015). Germline gain-of-function mutations in AFF4 cause a developmental syndrome functionally linking the super elongation complex and cohesin. Nat. Genet. *47*, 338–344.
15. Sovolyova, N., Healy, S., Samali, A., and Logue, S.E. (2014). Stressed to death - mechanisms of ER stress-induced cell death. Biol. Chem. *395*, 1–13.
16. Namba, T., Ishihara, T., Tanaka, K., Hoshino, T., and Mizushima, T. (2007). Transcriptional activation of ATF6 by endoplasmic reticulum stressors. Biochem. Biophys. Res. Commun. *355*, 543–548.
17. Oslowski, C.M., and Urano, F. (2011). Measuring ER stress and the unfolded protein response using mammalian tissue culture system. Methods Enzymol. *490*, 71–92.
18. Jiang, H., Jans, R., Xu, W., Rorke, E.A., Lin, C.-Y., Chen, Y.-W., Fang, S., Zhong, Y., and Eckert, R.L. (2010). Type I transglutaminase accumulation in the endoplasmic reticulum may be an underlying cause of autosomal recessive congenital ichthyosis. J. Biol. Chem. *285*, 31634–31646.
19. Consortium, E.A., Lek, M., Karczewski, K., Minikel, E., Samocha, K., Banks, E., Fennell, T., O'Donnell-Luria, A., Ware, J., Hill, A., et al. (2015). Analysis of protein-coding genetic variation in 60,706 humans. bioRxiv http://dx.doi.org/10.1101/030338.
20. Hoornaert, K.P., Vereecke, I., Dewinter, C., Rosenberg, T., Beemer, F.A., Leroy, J.G., Bendix, L., Björck, E., Bonduelle, M., Boute, O., et al. (2010). Stickler syndrome caused by COL2A1 mutations: genotype-phenotype correlation in a series of 100 patients. Eur. J. Hum. Genet. *18*, 872–880.
21. Sun, E., He, J., and Zhuang, X. (2013). Dissecting the role of COPI complexes in influenza virus infection. J. Virol. *87*, 2673–2685.
22. Boyadjiev, S.A., Kim, S.-D., Hata, A., Haldeman-Englert, C., Zackai, E.H., Naydenov, C., Hamamoto, S., Schekman, R.W., and Kim, J. (2011). Cranio-lenticulo-sutural dysplasia associated with defects in collagen secretion. Clin. Genet. *80*, 169–176.
23. Barat-Houari, M., Sarrabay, G., Gatinois, V., Fabre, A., Dumont, B., Genevieve, D., and Touitou, I. (2016). Mutation Update for COL2A1 Gene Variants Associated with Type II Collagenopathies. Hum. Mutat. *37*, 7–15.
24. Okada, M., Ikegawa, S., Morioka, M., Yamashita, A., Saito, A., Sawai, H., Murotsuki, J., Ohashi, H., Okamoto, T., Nishimura, G., et al. (2015). Modeling type II collagenopathy skeletal dysplasia by directed conversion and induced pluripotent stem cells. Hum. Mol. Genet. *24*, 299–313.
25. Rajpar, M.H., McDermott, B., Kung, L., Eardley, R., Knowles, L., Heeran, M., Thornton, D.J., Wilson, R., Bateman, J.F., Poulsom, R., et al. (2009). Targeted induction of endoplasmic reticulum stress induces cartilage pathology. PLoS Genet. *5*, e1000691.
26. Stephens, D.J., and Pepperkok, R. (2002). Imaging of procollagen transport reveals COPI-dependent cargo sorting during ER-to-Golgi transport in mammalian cells. J. Cell Sci. *115*, 1149–1160.

27. Zhang, X., Szabo, E., Michalak, M., and Opas, M. (2007). Endoplasmic reticulum stress during the embryonic development of the central nervous system in the mouse. Int. J. Dev. Neurosci. *25*, 455–463.
28. Ishikawa, T., Okada, T., Ishikawa-Fujiwara, T., Todo, T., Kamei, Y., Shigenobu, S., Tanaka, M., Saito, T.L., Yoshimura, J., Morishita, S., et al. (2013). ATF6α/β-mediated adjustment of ER chaperone levels is essential for development of the notochord in medaka fish. Mol. Biol. Cell *24*, 1387–1395.
29. Xu, X., Kedlaya, R., Higuchi, H., Ikeda, S., Justice, M.J., Setaluri, V., and Ikeda, A. (2010). Mutation in archain 1, a subunit of COPI coatomer complex, causes diluted coat color and Purkinje cell degeneration. PLoS Genet. *6*, e1000956.
30. Todd, A.G., Lin, H., Ebert, A.D., Liu, Y., and Androphy, E.J. (2013). COPI transport complexes bind to specific RNAs in neuronal cells. Hum. Mol. Genet. *22*, 729–736.
31. Gilchrist, A., Au, C.E., Hiding, J., Bell, A.W., Fernandez-Rodriguez, J., Lesimple, S., Nagaya, H., Roy, L., Gosline, S.J.C., Hallett, M., et al. (2006). Quantitative proteomics analysis of the secretory pathway. Cell *127*, 1265–1281.
32. Verrier, S.E., Willmann, M., Wenzel, D., Winter, U., von Mollard, G.F., and Söling, H.-D. (2008). Members of a mammalian SNARE complex interact in the endoplasmic reticulum in vivo and are found in COPI vesicles. Eur. J. Cell Biol. *87*, 863–878.
33. Ramakrishnan, N.A., Drescher, M.J., and Drescher, D.G. (2012). The SNARE complex in neuronal and sensory cells. Mol. Cell. Neurosci. *50*, 58–69.
34. Plácido, A.I., Pereira, C.M.F., Duarte, A.I., Candeias, E., Correia, S.C., Santos, R.X., Carvalho, C., Cardoso, S., Oliveira, C.R., and Moreira, P.I. (2014). The role of endoplasmic reticulum in amyloid precursor protein processing and trafficking: implications for Alzheimer's disease. Biochim. Biophys. Acta *1842*, 1444–1453.
35. Dupuis, N., Fafouri, A., Bayot, A., Kumar, M., Lecharpentier, T., Ball, G., Edwards, D., Bernard, V., Dournaud, P., Drunat, S., et al. (2015). Dymeclin deficiency causes postnatal microcephaly, hypomyelination and reticulum-to-Golgi trafficking defects in mice and humans. Hum. Mol. Genet. *24*, 2771–2783.
36. Baker, K., Gordon, S.L., Grozeva, D., van Kogelenberg, M., Roberts, N.Y., Pike, M., Blair, E., Hurles, M.E., Chong, W.K., Baldeweg, T., et al. (2015). Identification of a human synaptotagmin-1 mutation that perturbs synaptic vesicle cycling. J. Clin. Invest. *125*, 1670–1678.
37. Cafiero, C., Marangi, G., Orteschi, D., Ali, M., Asaro, A., Ponzi, E., Moncada, A., Ricciardi, S., Murdolo, M., Mancano, G., et al. (2015). Novel de novo heterozygous loss-of-function variants in MED13L and further delineation of the MED13L haploinsufficiency syndrome. Eur. J. Hum. Genet. *23*, 1499–1504.
38. Sobreira, N., Schiettecatte, F., Valle, D., and Hamosh, A. (2015). GeneMatcher: a matching tool for connecting investigators with an interest in the same gene. Hum. Mutat. *36*, 928–930.

**The American Journal of Human Genetics, Volume *99***

## Supplemental Data

# *ARCN1* Mutations Cause a Recognizable Craniofacial Syndrome Due to COPI-Mediated Transport Defects

**Kosuke Izumi, Maggie Brett, Eriko Nishi, Séverine Drunat, Ee-Shien Tan, Katsunori Fujiki, Sophie Lebon, Breana Cham, Koji Masuda, Michiko Arakawa, Adeline Jacquinet, Yusuke Yamazumi, Shu-Ting Chen, Alain Verloes, Yuki Okada, Yuki Katou, Tomohiko Nakamura, Tetsu Akiyama, Pierre Gressens, Roger Foo, Sandrine Passemard, Ene-Choo Tan, Vincent El Ghouzzi, and Katsuhiko Shirahige**

**Supplemental Information**

**Supplemental Note: Case Reports**

Subject 1 was referred to the Genetics Clinic of Nagano Children's Hospital at the age of 1 month with the chief complaints of facial dysmorphism and intrauterine growth retardation. Severe intrauterine growth retardation was noted during pregnancy. Subject 1 was born at 35 weeks gestation and was delivered by normal vaginal delivery. Her birth weight was 1100 gm (<3$^{rd}$ centile: -4.18SD), length was 34 cm (<3$^{rd}$ centile: -3.72SD), and head circumference was 26 cm (<3$^{rd}$ centile: -3.15SD). At birth, severe micrognathia and facial dysmorphism were noted. An echocardiogram revealed the presence of a ventricular septal defect. After birth, Subject 1 developed respiratory distress, requiring ventilator support. Severe micrognathia was considered to be the reason of respiratory distress. Therefore, when she was 6 months old, a tracheostomy was performed. The subsequent development of Subject 1 has been slightly delayed; she started standing with holding at 10 months and sitting independently at 11 months. At 1 year and 10 months, her developmental quotient (DQ) was 65. At the age of 3 years and 1 month, DQ for motor skills, cognition/adaptation, and language/social skills

were 75, 77, and 69, respectively. The overall DQ was 72. At the age of 3 years and 4 months, she recently met the developmental milestones of approximately 2 years and 6 months, since she was able to jump up, draw straight lines, and take off her clothes.

Since birth, she has continued to have short stature and has exhibited failure to thrive (Figure S1A). On physical examination, several facial dysmorphisms, including a prominent forehead, downslanted palpebral fissures, and severe micrognathia, were noted. In addition, shortening of upper arms and legs, and small joint laxity were observed (Figure 1A). Beighton score was 5/9. No skin color or hair abnormalities were identified. She has not shown any signs of cerebellar ataxia. A skeletal survey revealed widening of the metaphysis and a wide femoral neck (Figure 1B). Ophthalmological evaluation revealed astigmatism. Audiology evaluation was unremarkable. Brain MRI was also unremarkable. Currently, she is 3 years and 4 months old, and her height was 80.2cm (-4.1SD), weight was 8.8kg (-3SD), and head circumference was 43.4cm (-3.2SD). The family history of Subject 1 was unremarkable.

Subject 2, a boy with developmental delay and mild autism, was first seen in the Genetics Clinic, KK Women’s & Children’s Hospital, at the age of 1 year and 8

months. Antenatal scans showed intrauterine growth retardation, micrognathia, and possible ambiguous genitalia. Amniocentesis revealed a normal karyotype. Subject 2 was delivered at 34 weeks gestation via cesarean section and had a birth weight of 1360 gm (<3$^{rd}$ centile), birth length of 40cm (<3$^{rd}$ centile), and birth head circumference of 29cm (10$^{th}$ centile). Postnatally, it was observed that he had severe micrognathia and penoscrotal hypospadias and required tracheostomy for respiratory support during infancy (Figure S1B). He also developed severe gastroesophageal reflux, requiring fundoplication and gastrostomy insertion for the first 3 years of life. The development of Subject 2 was slightly delayed; he started walking independently at 13 months and climbing stairs at 18 months. He spoke his first words at 17 months. At 7 years of age, he has moderate-to-severe language difficulties and currently attends special education school. His medical issues include epilepsy and obstructive sleep apnea requiring continuous positive airway pressure support at night. An MRI scan of the brain of Subject 2 was normal and an electroencephalogram confirmed epileptiform activity. On physical examination, it was observed that Subject 2 had micrognathia, scaphocephaly, and hypotelorism, as well as small joint laxity (Figure 1C). Beighton score was 2/7. No

skin color or hair abnormalities identified. He has not shown any signs of cerebellar ataxia. The growth parameters of Subject 2 improved postnatally, and as of 7 years, his height is 121 cm, which is in the 10th centile. His mid-parental height is 172.5 cm, which is 50$^{th}$ centile. Currently he is 10 year and 6 months old, and his current height is 136cm (10th percentile) and weight 33.2kg (25th percentile), head circumference was 51cm (6$^{th}$ centile (-1.53SD)). His ophthalmological issues include occasional divergent squint and myopia. He does not have hearing problems.

Subject 3 (25 years old) was born at 36 weeks gestation from consanguineous parents (cousins): weight 1.450kg (<3$^{rd}$ centile), length 38cm (<3$^{rd}$ centile), head circumference 27.6 cm (<3$^{rd}$ centile). Hypotelorism, micrognathia, short bowed legs, and high arched palate were noticed at birth. Bilateral posterior cataract was diagnosed when he was 6 years old. He had hypertrophic muscular appearance, rhizomelic shortness of upper and lower limbs, large hands and feet, micropenis, and hypoplastic scrotum. A skeletal survey at 7 years of age demonstrated short femoral and humeral diaphysis, thick femoral neck with coxa valga, and advanced wrist bone maturation. The Subject 3's IQ was rated at 65 based on the Wechsler Intelligence

Scale for Children (WISC). At the age of 25 years, his weight was 98kg, his length was 152cm (-3.5 SD), and his head circumference was 50 cm (-5 SD) (Figure 1D). He cannot read or write but can be understood. He is an employee in his father's company and has married a woman from another region.

Subject 4, the daughter of Subject 3, shared common features with Subject 3, which included intrauterine growth retardation followed by postnatal growth failure. Currently, she is 3 years old, and her height was 79.5 cm (-4 SD), her weight was 9.650kg (-3SD) and head circumference was 45 cm (-5 SD). She was also found to have dysmorphic features including microretrognathia, hypotelorism, shortening of upper arms and legs, and muscular hypertrophy (Figure 1E). Subject 4 was born at term: weight 1.400kg (<3$^{rd}$ centile), length 37cm (<3$^{rd}$ centile), head circumference 27.5cm (<3$^{rd}$ centile). She had a cleft palate, and feeding difficulties that required nutritional support until the age of 2 years. She started walking at 2 years of age with ataxia, and she does not speak yet. Her brain MRI showed microcephaly, delayed white mater myelination in T2 weight images, and mild cerebellar atrophy (Figure S1C).

Exome sequencing was performed for Subject 1 as well as her unaffected

biological parents. The G-band karyotype and SNP array results were normal. Exome capture was performed with Agilent SureSelect XT Human All Exon V5 (Agilent, Santa Clara, Calif., USA), and 100-bp or 126-bp paired-end read sequencing was performed by HiSeq 2500 (Illumina, San Diego, Calif., USA). The sequenced reads were aligned to the human genome hg19 using BWA v0.7.12 with BWA-MEM algorithm and '-M' option[1]. The Genome Analysis Toolkit (GATK) v3.3.0 was used for variant discovery[2]. After marking duplicates, local realignment around indels, and base quality score recalibration, SNVs and indels for each sample were called using the HaplotypeCaller. SNVs and indels with a GQ score above 15 were used for further analysis. The effects of variants were predicted by SnpEff v3.6b[3] and annotated by ANNOVAR[4]. Information and statistics regarding sequenced reads, mapping rate, and coverage are summarized in Table S1. Six *de novo* mutations in 4 genes (*ARCN1*, *DCAF15*, *HLA-DRB5*, *FAM58A*) were identified. However, variants in *DCAF15*, *HLA-DRB5,* and *FAM58A* were present in dbSNP, leaving *ARCN1* as the prime candidate gene to account for the subject's phenotype. The mutation in *ARCN1* resulted in a premature stop codon in exon 2 (NM_001655:exon2:c. 260C>A:p.Ser87*). The *ARCN1* mutation was confirmed by

Sanger sequencing (Figure 2A and Figure S2A). Sanger sequencing demonstrated that the *DCAF15* variant was inherited from her unaffected father and the *FAM58A* variants were inherited from her unaffected parents (Figure S3A and S3B).

Subject 2 was independently identified in a cohort of individuals from Singapore with undiagnosed genetic diseases. He had been previously tested and his karyotype and chromosome microarray analysis results were normal. Exome sequencing of Subject 2 and his unaffected parents was carried out by the Genome Institute of Singapore using the NimbleGen SeqCap EZ Human exome V3 kit (Roche, Basel Switzerland) and sequenced on the HiSeq 2000 platform (Illumina, San Diego, USA) using 100-bp paired-end reads. Alignment to the human genome hg19 was carried out using BWA 0.7.5a and the variants were annotated using ANNOVAR. Variants with minor allele frequency (MAF) >0.01 in dbSNP or EVS (Exome Variant Server) were excluded and rare functional variants were prioritized according to *de novo* status, homozygosity, compound heterozygosity and X chromosome-linkage. After filtration, *de novo* heterozygous variants were identified in *ARCN1* and *SYT1*. Both of these variants were confirmed by Sanger sequencing. The *ARCN1* mutation was a

frameshift variant: NM_001655:c.633del; p.Val212Trpfs*15 predicted to create a frameshift in exon 4 starting at codon Val212 and ending in a stop codon 14 positions downstream (Figure 2A and Figure S2B). The *SYT1* (NM_001135805.1:c.697G>A; p.Asp233Asn) variant is a missense variant that substitutes Aspartic acid at codon 233 with Asparagine (Figure S3C). There were no other potentially pathogenic mutations.

Subjects 3 and 4 were also ascertained independently. Whole-exome sequencing was performed for Subject 3 and his healthy parents by IntegraGen Genomics. Exons of DNA samples were captured using an in-solution enrichment methodology (Agilent SureSelect All Exon V4 + UTRs) and sequenced with an Illumina HiSeq 2000 instrument. SNPs and indels were determined using the CASAVA 1.8 software. Identification of the disease-causing variants was performed with the Exome Resequencing Intelligent Sorter (ERIS, Integragen) program for the annotation and filtering of genetic variants. The following criteria were used for excluding non-pathogenic variants: (1) variants represented with an allele frequency of more than 0.5% in dbSNP 138, the NHLBI Exome Sequencing Project EVS, or the in-house database of Integragen; (2) variants in the 5’ or 3’ UTR; (3) variants with intronic

locations and no prediction of local splice effect; and (4) synonymous variants without prediction of local splice effect. Filtered variants occuring *de novo* were retained for further confirmation and segregation analysis by Sanger sequencing. The *ARCN1* mutation was the only probably damaging mutation that occurred *de novo* in Subject 3 and was transmitted to his affected daughter, Subject 4. The *ARCN1* mutation was NM_001655:c.157_158del, leading to p.Ser53Cysfs*39 (Figure S2C).

**Supplementary Figures**

**Figure S1.** Additional clinical information of the individuals with *ARCN1* mutations. (A) Growth chart of Subject 1. Green dots represent height measurements, red dots represent weight measurements, and blue dots represent head circumference measurements. (B) Radiograph of Subject 2 demonstrating the presence of micrognathia. (C) Brain MRI of Subject 4. Microcephaly with gyral simplification, thin corpus callosum, delayed myelination and mild cerebellar atrophy are demonstrated.

(A)

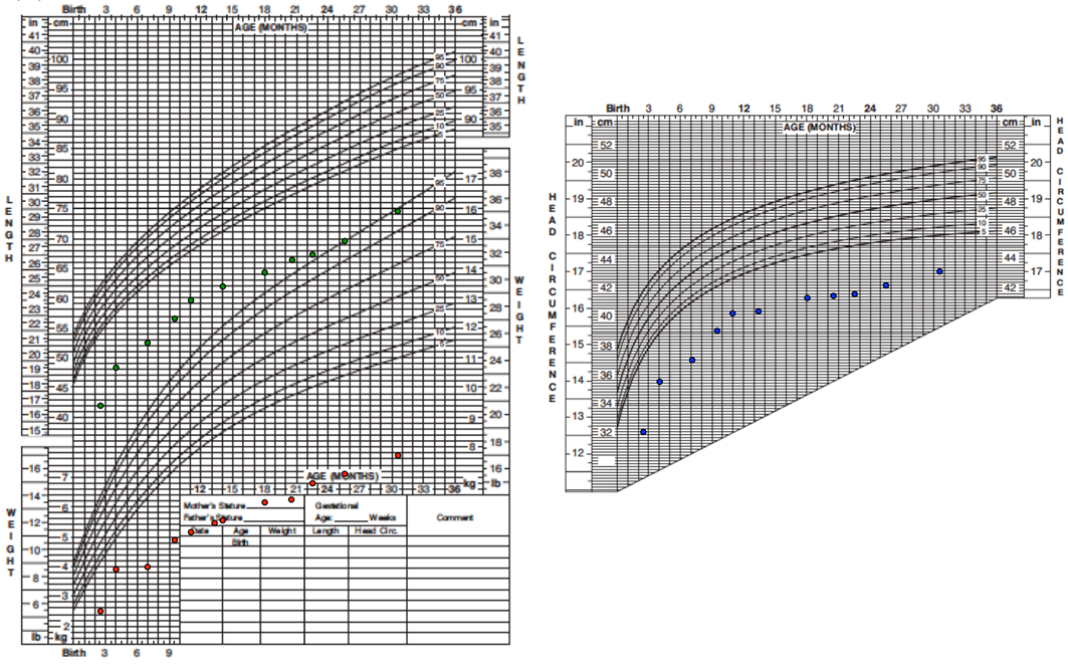

(B)

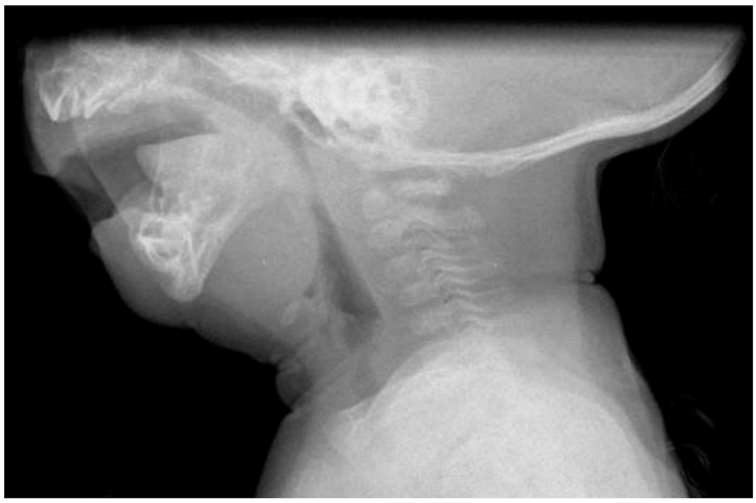

(C)

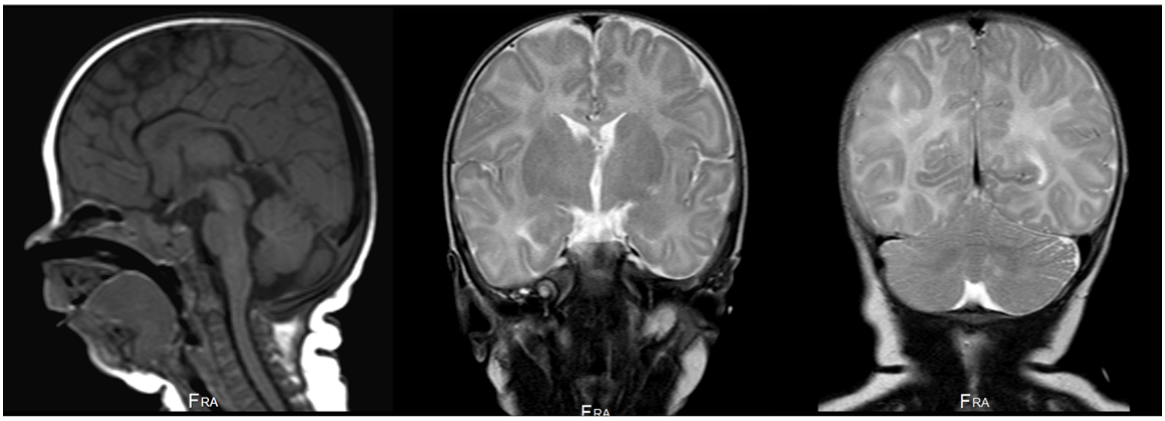

**Figure S2.** Sanger sequencing chromatogram of *ARCN1* mutations. (A) *ARCN1* mutation in Subject 1. Neither of the parents carried the same mutation. (B) *ARCN1* mutation in Subject 2. Neither of the parents carried the same mutation. (C) *ARCN1* mutation in Subjects 3 and 4. *ARCN1* mutation was not detected in the parents of Subject 3. (D) *ARCN1* mutations introduced by CRISPR/Cas9 in HCT116 cell line clones.

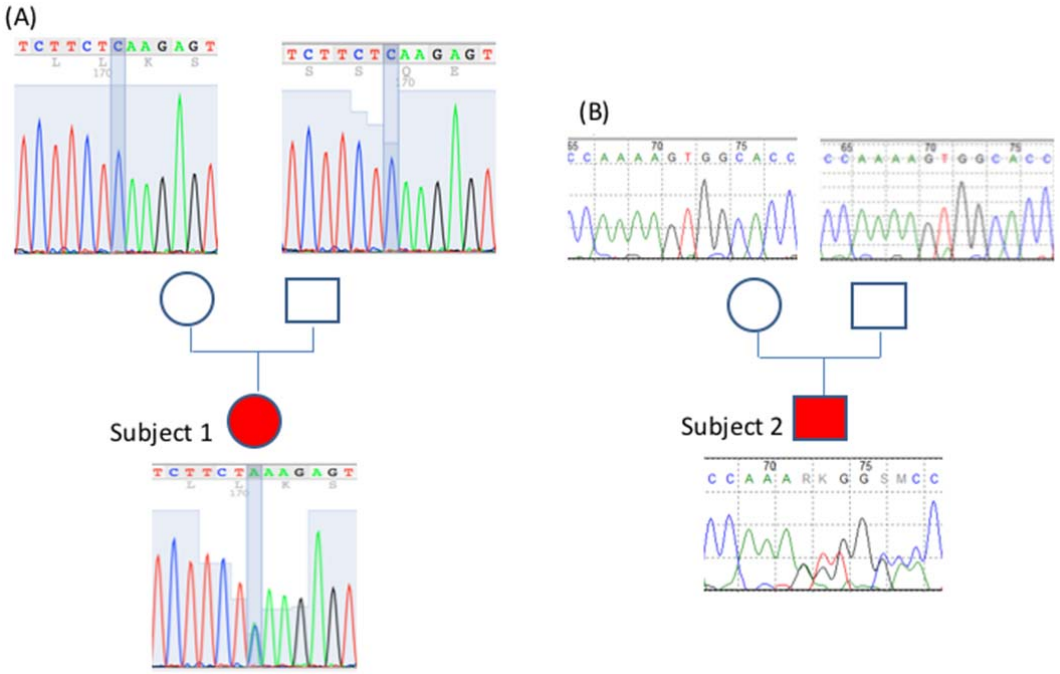

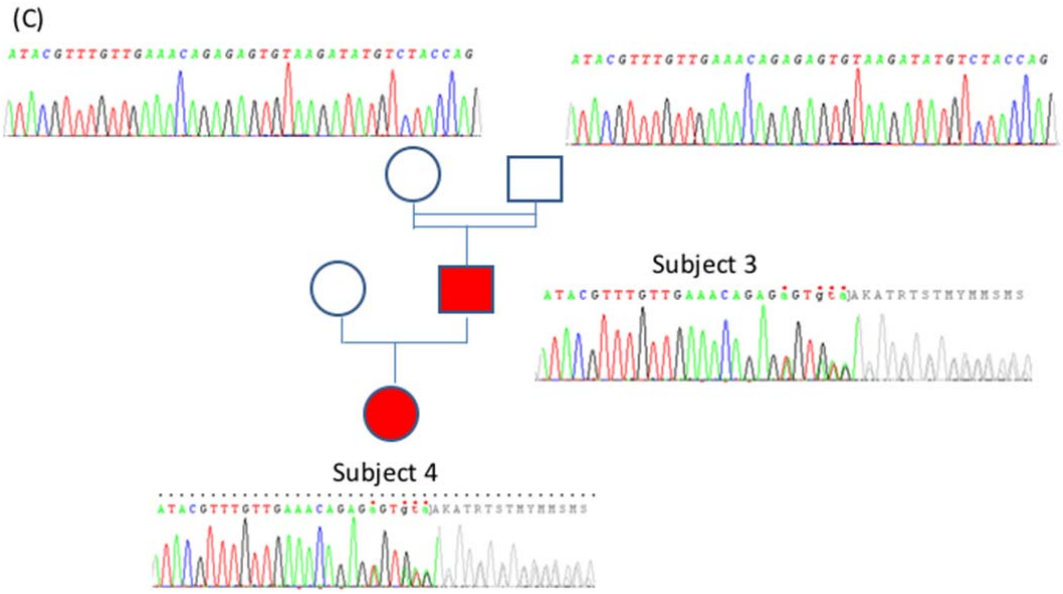
(C)
Subject 3
Subject 4

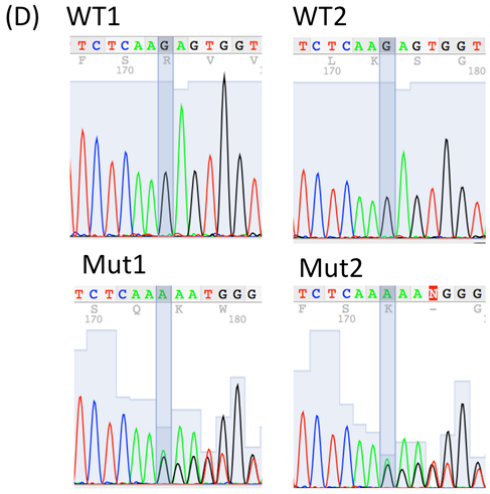
(D)
WT1
WT2
Mut1
Mut2

**Figure S3.** Sanger sequencing confirmation of *FAM58A*, *DCAF15* and *SYT1* variants. (A) The *FAM58A* variant was identified not only in Subject 1, but also in both parents, arguing against a possible role of the *FAM58A* variant in explaining the clinical phenotype of Subject 1. This variant was reported in dbSNP as rs200645137, and its population frequency is between 0.987 and 1.0 in the Human Genetic Variation database (http://www.genome.med.kyoto-u.ac.jp/SnpDB/index.html). (B) The *DCAF15* variant was confirmed in Subject 1, but the same variant was also identified in her father, arguing against its causality. A similar insertion was reported in dbSNP as rs3217681, and its population frequency is 0.407 according to the Human Genetic Variation database. (C) The *SYT1* variant in Subject 2 was confirmed by Sanger sequencing, and neither parent was found to have this variant. This *SYT1* variant represents a novel variant, and has not been previously reported in the public SNV database.

(A) *FAM58A* Sanger sequencing

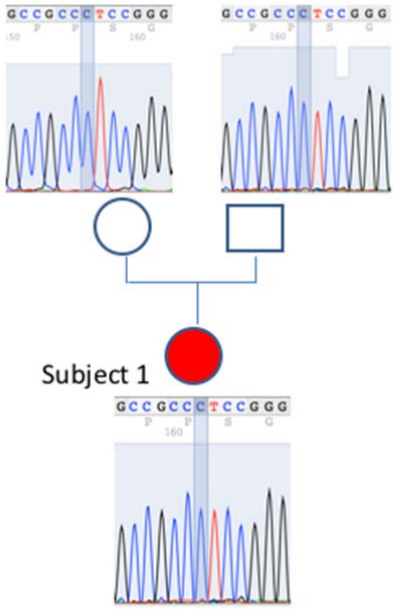


*FAM58A*: NM_152274: c.16_17ins G

(B) *DCAF15* Sanger sequencing

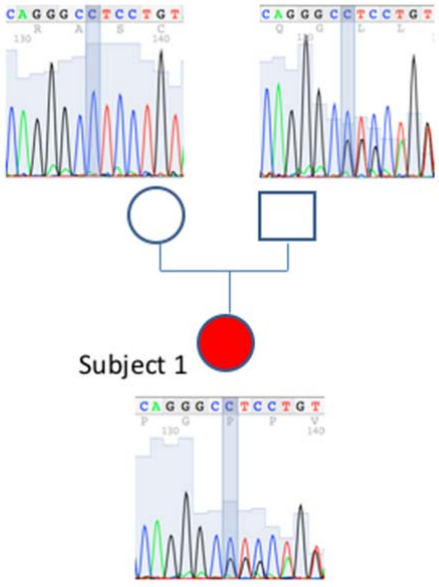


*DCAF15*:NM_138353:c.1439_1440insGGTGGGCCCAGGGCGGGCAG:p.E480fs

(C) *SYT1* Sanger sequencing

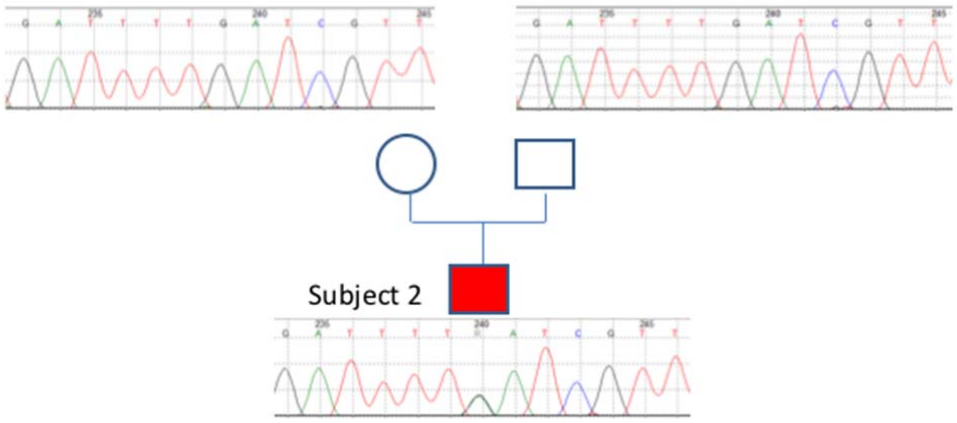


*SYT1*: NM_001135805.1:c.697G>A

**Figure S4.**Quantitative RT-PCR and western blot using *ARCN1*-related syndrome subject-derived skin fibroblast samples. (A) Quantitative RT-PCR. Total RNA was extracted from fibroblasts with the RNeasy Mini Kit according to the manufacturer's instructions (Qiagen, Courtaboeuf, France). Total RNA was subjected to reverse transcription using the iScript cDNA synthesis kit (Bio-rad, Marnes la Coquette, France). qPCR was performed in duplicate for each sample using the SybrGreen Supermix (Bio-rad). The relative expression of *ARCN1* was expressed relative to the expression of *HPRT*. The *ARCN1* expression level was significantly reduced in samples from Subjects 3 and 4 compared to that of the control sample. *** P<0.001, one-way ANOVA followed by a Bonferroni post-test. Error bars represent standard error of the mean. Two replicates were performed. (B) and (C) ARCN1 and BiP western blotting. Whole cell extracts were fractionated by SDS-PAGE and transferred to a polyvinylidene difluoride (PVDF) membrane. After incubation with 10% nonfat milk in TBST (10 mM Tris, pH 8.0, 150 mM NaCl, 0.5% Tween 20) for 1 h, membranes were incubated with antibodies against ARCN1 (COP1D, AV54594, Sigma-Aldrich), BiP (Grp78, ab21685, Abcam) or beta-Actin (MAB1501, Millipore) overnight at 4 °C. Membranes were washed three

times and incubated with horseradish peroxidase-conjugated anti-mouse or anti-rabbit antibodies. Blots were washed with TBST and developed with the ECL system (Amersham Biosciences) according to the manufacturer's protocols. (B) The protein level of ARCN1 was slightly reduced in the Subject 4 sample, compared to that of the control sample. Two replicates demonstrated consistent results. (C) Western blotting with BiP antibody yielded two bands, and lower band representing BiP based on the molecular size (about 78kDa). The BiP protein, which is an ER stress marker, was elevated in the Subject 4 sample, compared to that of the control.

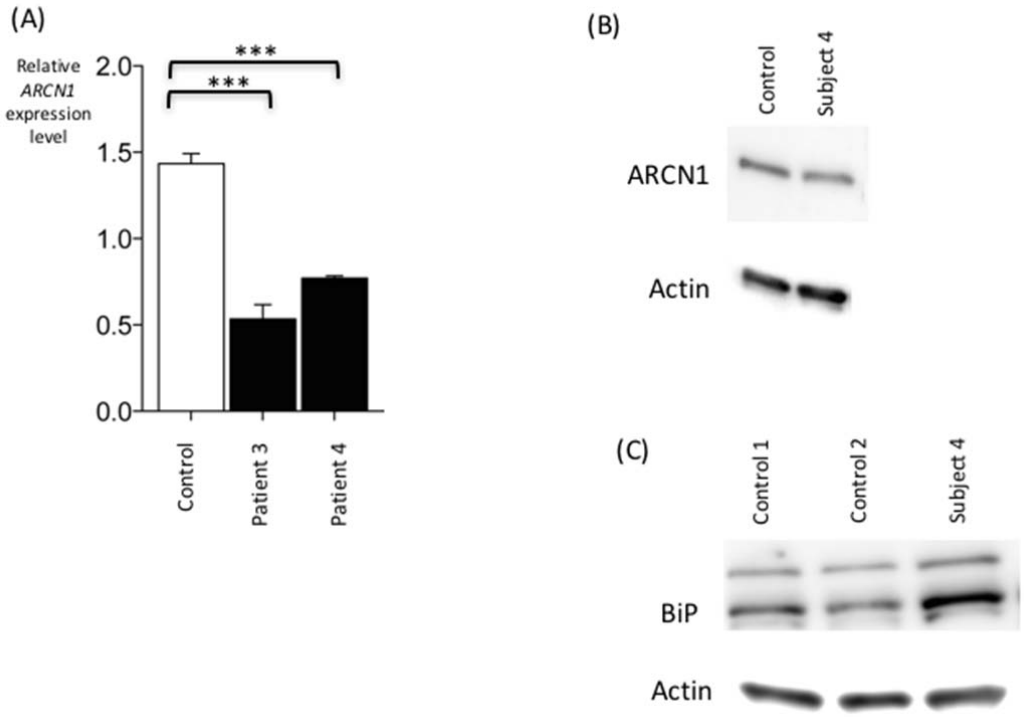

**Figure S5.** Immunocytochemical analysis. Cultures were fixed for 20 min with 4% paraformaldehyde. For immunocytochemistry, the cells were permeabilized with 0.3% TritonX-100 for 15min, washed, blocked for 1 h with 10% serum in PBS and incubated with primary antibody overnight at 4°C. Primary antibodies used were anti-ARCN1/COP1D (ab96725, Abcam), anti-GM130 (610823, BD Transduction Lab), anti-GIANTIN (ab80864, Abcam), and anti-PDI (MA3-019, Thermofisher). Following washing, cells were treated with secondary antibody for 1 h in the dark at room temperature. All images were captured on a Zeiss microscope IMAGER.Z1, using the Apotome imaging system coupled to AxioCam MRm and the Axiovision Rel.4.8 software. BiP represents an ER stress marker, and GIANTIN and GM130 are Golgi markers. PDI is a marker of ER. Immunofluorescence staining of the Golgi apparatus (GIANTIN and GM130), and that of ER (PDI) as well as COPI vesicle (ARCN1) indicated the swollen appearance of the Golgi stacks in the Subject 4's fibroblast. Accumulation of BiP in the cytosol is demonstrated in the Subject 4's fibroblast compared to that of the control.

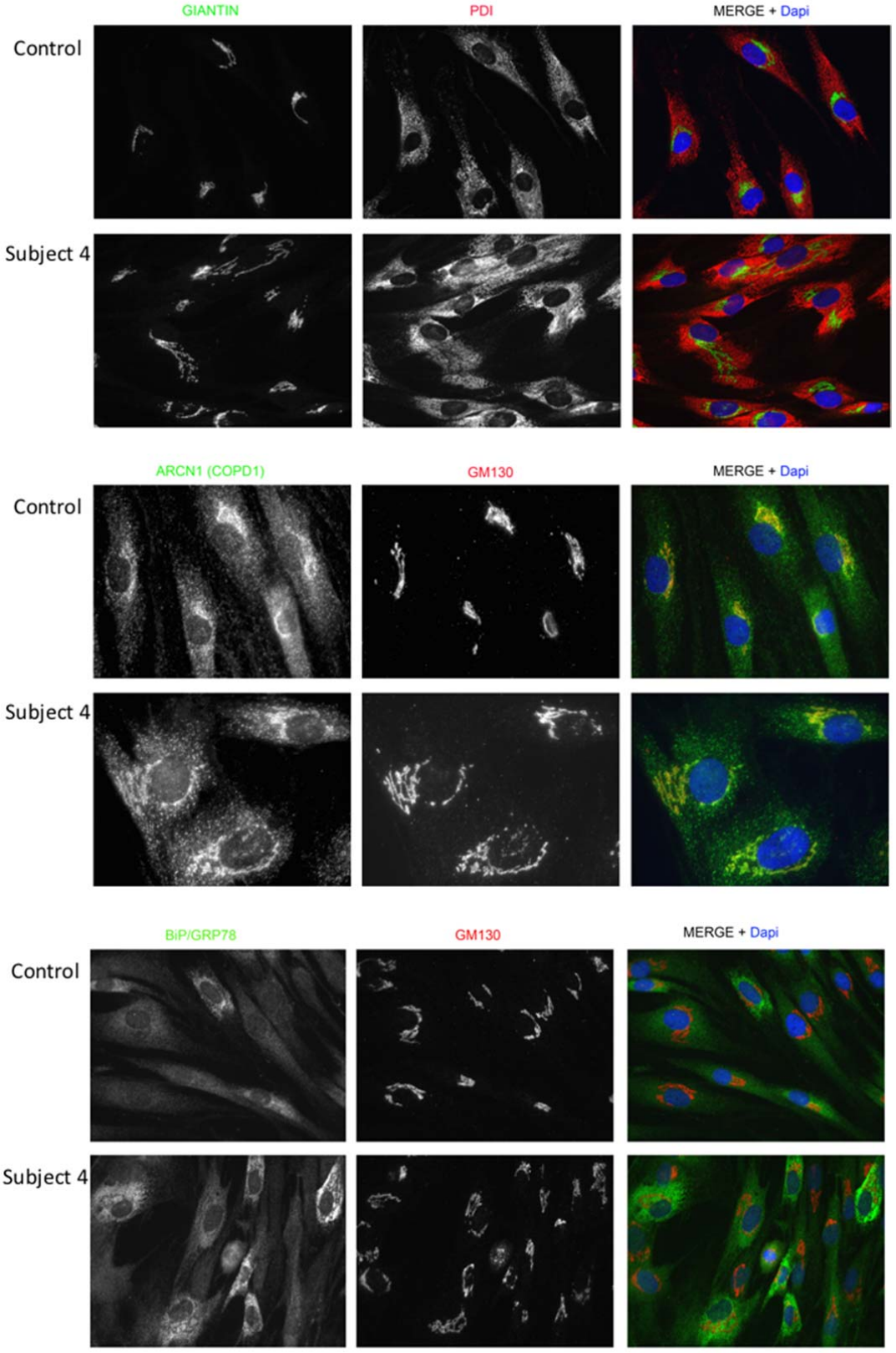
GIANTIN
PDI
MERGE + Dapi
Control
Subject 4
ARCN1 (COPD1)
GM130
MERGE + Dapi
Control
Subject 4
BiP/GRP78
GM130
MERGE + Dapi
Control
Subject 4

**Figure S6.** ER stress gene expression was elevated with tunicamycin and thapsigargin treatments. Data represents mean ± 2 s.d. *** P<0.001, two-tailed *t* test; n=3 technical replicates per group. Quantitative PCR was run in triplicates, and mean and standard deviation was calculated. Two different concentrations of tunicamycin treatment (2µg/ml (Tuni2) and 5µg/ml (Tuni5)) and thapsigargin treatment (2µM (Tg2) and 5µM (Tg5)) were used. DMSO was added for control. Gene expression level was normalized against *GAPDH* expression. Relative gene expression level to the control sample is demonstrated.

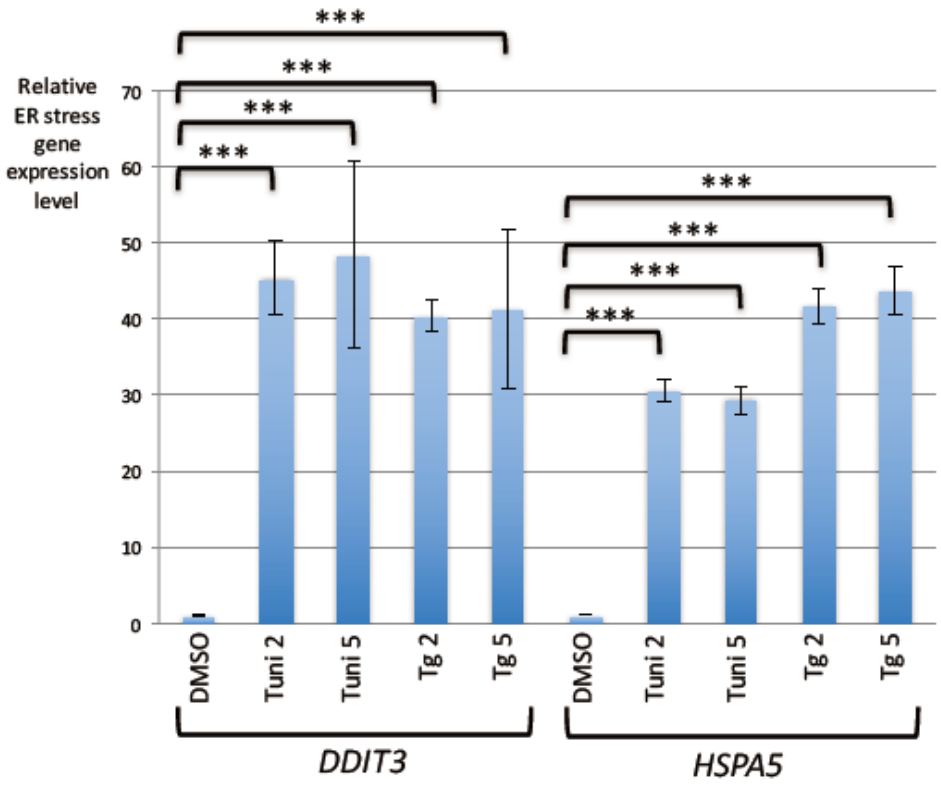

**Table S1. Exome statistics**

| sample name | platform | read length (bp) | read type | method | total reads | mapped reads | mapping rate (%) | mapping tool |
|---|---|---|---|---|---|---|---|---|
| Subject 1 | Hiseq 2500 | 100 or 126 | paired-end | Exome sequencing | 134459385 | 134274949 | 99.86 | BWA 0.7.12 |
| Subject 1 Father | Hiseq 2500 | 100 or 126 | paired-end | Exome sequencing | 138379220 | 138209817 | 99.88 | BWA 0.7.12 |
| Subject 1 Mother | Hiseq 2500 | 100 or 126 | paired-end | Exome sequencing | 136127612 | 135820259 | 99.77 | BWA 0.7.12 |
| Subject 2 | Hiseq 2000 | 100 | paired-end | Exome sequencing | 121420265 | 120842553 | 99.52 | BWA 0.7.5a |
| Subject 2 Father | Hiseq 2000 | 100 | paired-end | Exome sequencing | 112431640 | 112118195 | 99.72 | BWA 0.7.5a |
| Subject 2 Mother | Hiseq 2000 | 100 | paired-end | Exome sequencing | 111109537 | 110800648 | 99.72 | BWA 0.7.5a |

| | | | | | | | | |
|---|---|---|---|---|---|---|---|---|
| Subject 3 | Hiseq 2000 | 75 | paired-end | Exome sequencing | 70427250 | 68814466 | 97.71 | ELANDv2e |
| Subject 3 Father | Hiseq 2000 | 75 | paired-end | Exome sequencing | 73368174 | 71746737 | 97.79 | ELANDv2e |
| Subject 3 Mother | Hiseq 2000 | 75 | paired-end | Exome sequencing | 50373665 | 49265444 | 97.8 | ELANDv2e |

Read information for Subjects 1, 2 and 3

| sample Name | mean | proportion of bases above 10X coverage (%) | proportion of bases above 20X coverage (%) | proportion of bases above 30X coverage (%) | proportion of bases above 50X coverage (%) |
|---|---|---|---|---|---|
| Subject 1 | 200.67 | 99.6 | 99.1 | 98.3 | 95.4 |
| Subject 1 Father | 208.9 | 99.7 | 99.1 | 98.3 | 95.4 |
| Subject 1Mother | 194.82 | 99.6 | 99.1 | 98.2 | 95.2 |
| Subject 2 | 99.96 | 96 | 93 | 89 | 76 |
| Subject 2 Father | 91.96 | 95 | 93 | 88 | 72 |
| Subject 2 Mother | 90.95 | 95 | 92 | 87 | 71 |

| sample Name | mean depth (X) | proportion of bases above 1X coverage (%) | proportion of bases above 4X coverage (%) | proportion of bases above 10X coverage (%) | proportion of bases above 25X coverage (%) |
|---|---|---|---|---|---|
| Subject 3 | 72 | 99 | 97 | 93 | 82 |
| Subject 3 Father | 77 | 99 | 97 | 93 | 83 |
| Subject 3 Mother | 58 | 99 | 96 | 91 | 77 |

Coverage information for Subjects 1,2 and 3

**Table S2**. Quantitative RT-PCR primers

| | F | R |
|---|---|---|
| *GAPDH* | GCACCGTCAAGGCTGAGAAC | TGGTGAAGACGCCAGTGGA |
| *HPRT* | GGTGAAAAGGACCCCACG | TCAAGGGCATATCCTACAACA |
| *ARCN1 ex9-10* | CGAAATACCCTGGAGTGGTG | GGGGCTGTTTCCATCTACCT |
| *ARCN1 ex1-2* | TCCCGTTCCCCAGACCCTA | TTTCCTGCTTTTGTGCAGAC |
| *ATF4* | TCAAACCTCATGGGTTCTCC | GCATGGTTTCCAGGTCATCT |
| *DDIT3* | GACCTGCAAGAGGTCCTGTC | AGGTGCTTGTGACCTCTGCT |
| *HSPA5* | TGAAACTGTGGGAGGTGTCA | TTTGTCAGGGGTCTTTCACC |
| *COL1A1* | GACTGGCAACCTCAAGAAGG | GGAGGTCTTGGTGGTTTTGT |
| *COL1A2* | GCAACCTGAAAAAGGCTGTC | GGCGTGATGGCTTATTTGTT |

*ARCN1* ex9-10 primer pair was used for HCT116 cell lines, and *ARCN1* ex1-2 primer pair was used for skin fibroblast cell lines.

**Table S3. Comparison of *SYT1* mutation cases**

| Subject | *SYT1* variant | Variant effect prediction | | | Clinical phenotype | | | | |
|---|---|---|---|---|---|---|---|---|---|
| | | Polyphen2 HumDiv | SIFT | Mutation taster | Developmental delay | Movement disorder | Seizure | Micrognathia | IUGR |
| Subject 2 (Current report) | c.697G>A; p.Asp233Asn | Probably damaging | Tolerated | Disease causing | Mild | No | Yes | Yes | Yes |
| Baker et al.(2015) J. Clin. Invest. 125, 1670–1678. | c.1103T>C; p.Ile368Thr | Benign | Tolerated | Disease causing | Profound | Yes | No | No | No |
| Cafiero et al.(2015) Eur. J. Hum. Genet. 23, 1499–1504. | c.908T>A; p.Met303Lys | Benign | Damaging | Disease causing | Moderate | No | No | No | No |

**Supplementary References**

1. Li, H., and Durbin, R. (2009). Fast and accurate short read alignment with Burrows-Wheeler transform. Bioinforma. Oxf. Engl. *25*, 1754–1760.
2. DePristo, M.A., Banks, E., Poplin, R., Garimella, K.V., Maguire, J.R., Hartl, C., Philippakis, A.A., del Angel, G., Rivas, M.A., Hanna, M., et al. (2011). A framework for variation discovery and genotyping using next-generation DNA sequencing data. Nat. Genet. *43*, 491–498.
3. Cingolani, P., Platts, A., Wang, L.L., Coon, M., Nguyen, T., Wang, L., Land, S.J., Lu, X., and Ruden, D.M. (2012). A program for annotating and predicting the effects of single nucleotide polymorphisms, SnpEff: SNPs in the genome of Drosophila melanogaster strain w1118; iso-2; iso-3. Fly (Austin) *6*, 80–92.
4. Wang, K., Li, M., and Hakonarson, H. (2010). ANNOVAR: functional annotation of genetic variants from high-throughput sequencing data. Nucleic Acids Res. *38*, e164.